JBUON 2016; 21(3): 633-644
ISSN: 1107-0625, online ISSN: 2241-6293 • www.jbuon.com
E-mail: editorial_office@jbuon.com

ORIGINAL ARTICLE

Silybin nanoparticles for liver cancer: development, optimization and *in vitro* – *in vivo* evaluation

Han Zhang[1], Cheng-Bao Wang[2], Jin-Ling Liu[1]

[1]Department of Spleen and Stomach and [2]Department of Infectious Diseases, Chinese Medicine Hospital in Linyi City, Linyi 276000, China

Summary

Purpose: *Hepatocellular carcinoma (HCC) is a most common liver malignancy. The objective of this study was to prepare silybin nanoparticles (NPs) and optimize the prepared nanoparticles using central composite rotatable design-response surface methodology.*

Methods: *HCC was induced in rats by supplementing 100 mg/L of diethylnitrosamine (DENA) in drinking water for 8 weeks. Saline, silybin 30 mg/kg body weight and nanoformulation of silybin equivalent to silybin dose were administered orally to 3 groups of 6 animals each. Anticancer activity was evaluated by counting the liver nodules, and H & E staining analysis of tissue sections.*

Results: *The results showed that silybin NPs under optimized conditions gave rise to the entrapment efficiency (EE) of 88%, drug loading (DL) of 15%, mean diameter of 216 nm of the NPs prepared and zeta potential value of -15 mV. In rats treated with silybin NPs, the number of neoplastic nodules was significantly lower, the animals did not exhibit decrease in mean body weight, the number of liver nodules was reduced by >93% with significantly high localization in the liver.*

Conclusion: *Orally administered silybin NPs showed improved efficacy and safety compared to silybin for the treatment of HCC in rats.*

Key words: *drug delivery, hepatocellular carcinoma, nanoparticles, oral chemotherapy, response surface methodology, silybin*

Introduction

With over 660,000 new cases and 630,000 resultant deaths estimated in 2009, primary liver cancer or HCC, is the fifth most prevalent malignancy and the third leading cause of cancer-related deaths worldwide [1-3]. Although 80% of the cases occur in regions where hepatitis B infection is endemic, the incidence of HCC is rising at epidemic proportions as a result of the rampant spread of hepatitis C in the 1950s and 1960s [2-4]. HCC is a highly lethal disease, as demonstrated by the equal annual incidence and mortality, and the dismal 8-month median survival without treatment [5] is improved only by a modest 3 months when the best systemic therapy available, sorafenib, is employed [6]. On the contrary, when HCC is detected at an early stage, curative treatments such as surgical resection, liver transplantation, and ablative therapies can be used, achieving 5-year survival rates of up to 75%, highlighting the importance of early detection [7-9].

Diagnosis of early-stage HCC is heavily dependent on quality multiphase, contrast-enhanced computed tomography (CT) and magnetic resonance imaging (MRI), current gold standards [10]. Although characteristic arterial enhancement with portal venous washout of a liver lesion on CT or MRI is diagnostic for HCC, undetermined lesions are frequently detected [10,11] prompting costly repeat imaging or biopsies with bleeding or tumor-seeding risks [12,13], all resulting in delay of diagnosis and treatment. Furthermore, eligibility for surgical resection or liver trans-

Correspondence to: Jin-Ling Liu, Med.Bach. Department of Spleen and Stomach, Chinese Medicine Hospital, Linyi City, No. 211 Jiefang Road, Lanshan District, Linyi, Shandong 276000, China. Tel & Fax: +86 539 8215177, E-mail: jinlingliu1976@gmail.com
Received: 20/05/2015; Accepted: 20/10/2015

plantation based on suboptimal scans leads to early recurrences and poor outcomes or missed treatment opportunities.

Several NP systems are being investigated for use in cancer diagnostics and therapeutics [14-17]. HCC targeting with NPs remains challenging as Kupffer cells, specialized macrophages dispersed throughout liver sinusoids that comprise an elaborate reticuloendothelial system (RES), take up these particles and interfere with the imaging or delivery of therapeutic payloads [17-19]. Much effort has been devoted to optimizing selective delivery of NPs to tumors while evading the RES, using surface modification of NPs with antifouling polymers such as polyethylene glycol (PEG) and various tissue-specific ligands [20,21]. Strategies that identify HCC-specific cell surface moieties to conjugate to achieve superior specificity hold the most promise. Vascular endothelial growth factor, epidermal growth factor receptor and small molecules such as galactose have been reported as potential targeting moieties for specific delivery of NPs and drugs to HCC cells [22-25]. However, the demand for novel targeting ligands for HCC-specific delivery remains high as no single receptor is uniformly expressed by the heterogeneous population of HCCs, and the efficiency of existing HCC-targeting ligands is less than ideal. Furthermore, a two-step pre-targeting approach to further enhance the signal for antibody-targeted imaging and treatment has been reported [26,27].

Silybin is one of the oldest drugs considered for the treatment of liver cancer. Although it is considered to be ideal for the treatment of liver cancer, delivery to the liver still needs improvement. Silybin needs to be administered daily to achieve its effects. Nanosized carriers encapsulating silybin can be taken up passively into Kupffer cells in the liver and can result in increased drug concentration in the liver, thus increasing the therapeutic efficacy. They can result in sustained systemic release of sylibin for more than a week, depending on various factors, after forming a depot in the Kupffer cells. Thus, repeated daily administration for sylibin can be avoided. Furthermore, oral bioavailability problems with sylibin can be avoided since bioavailability is significantly higher following the administration of nanoformulations.

On the other hand, oxidative stress in Kupffer cells is known to initiate the formation of liver fibrosis in many diseases and thus sylibin levels in these cells, if enhanced, can tremendously improve therapy with sylibin. Thus, with this type of formulation, sustained release, improvement in bioavailability as well as enhancement of biochemical protection can be achieved. Together, these mechanisms lead to increased effectiveness of therapy.

Thus, the objective of this study was to prepare and optimize the biodegradable NPs of silybin, and to evaluate their characteristics like particle size, surface morphology, zeta potential, EE and drug loading efficiency and finally liver targetability and anticancer efficacy following oral administration of nanoformulation of silybin.

In addition, the effects of drug/lipid ratio (X1), organic/aqueous phase ratio (X2) and sonication time (X3) on the EE, drug loading (DL) percentage and mean particle size (PS) of silybin NPs were investigated in detail making use of central composite rotatable design (CCRD) which is an ideal tool for process optimization [28,29]. Model equations were derived by computer simulation programming Design Expert ® 8.0.7.1 to optimize silybin nanostructured lipid carrier (NLC). For better understanding of the three variables, the models were presented as three dimensional (3D) response surface graphs.

Methods

Silybin, Poly-ε-caprolactone (mol wt., 14,000), Polyvinyl alcohol (PVA, cold-water soluble) and Dichloromethane were procured from Sigma-Aldrich, Germany. All other reagents were of analytical grade. Male Wistar rats weighing 150-180 g were obtained from the animal house of Chinese Medicine Hospital, Shandong, China.

Cell culture

A murine transplantable T-cell lymphoma of spontaneous origin, designated as Dalton's lymphoma (DLy), was used as a tumor model. This tumor was initially originated in the thymus gland of a DBA/2 mouse at the National Cancer Institute, Bethesda, USA, in 1947 and afterwards serially transplanted in the intraperitoneal cavity from mouse to mouse [30].

DLy cells harvested from DLy-bearing mice were cultured in RPMI-1640 medium supplemented with 10% FBS and antibiotic solution (penicillin 1000 IU and streptomycin 10 mg/mL) in 5% CO_2 incubator at 37 °C.

Animal model

For *in vivo* studies Swiss albino mice were housed in well-ventilated cages and fed with standard mouse feed and water *ad libitum*. The animals were acclimatized to standard environmental conditions of temperature (22°C ±5) for 12 hrs light-dark cycles throughout

the experimental period. The animals used for the study were approved by the central animal ethics committee (CAEC) of the University.

Tumor model

The anticancer effect of the silybin NPs was determined on DLy, for which ascites tumor was maintained in mice. Cells (1×10^6/mL) were transplanted in the peritoneal cavity of the mice. Dalton's lymphoma ascites (DLyA) cells can propagate as transplantable ascites tumor in Swiss albino mice.

Isolation of mouse bone marrow cells

Bone marrow cells were isolated from femur bones of approximately 8-10 week old mice by dislocation after mild anaesthesia exposure. The bone marrow was flushed with pre-warmed phosphate buffer saline (PBS) through a 24-gauge needle and single cell suspension was prepared by agitation. The cell suspension was centrifuged at 1500 rpm for 5 min.

The cells were finally resuspended in RPMI-1640 medium supplemented with 10% FBS and antibiotic solution. Cells were seeded in culture plates with supplemented RPMI-1640 medium and maintained in 5% CO2 at 37 °C for 24 hrs for the experiment.

Preparation of silybin nanoparticles

Emulsion (o/w) solvent evaporation method was employed in the preparation of silybin NPs using poly-ε-caprolactone as the polymer. For the preparation, silybin (100 mg) and polycaprolactone (100, 200, 300 or 400 mg) were dissolved in 15 ml of dichloromethane by vortexing. The mixture (organic phase) was added drop-wise to 50 ml of 2% PVA solution under probe sonication at 40 w for 10 min to obtain a o/w emulsion. This emulsion was placed on a magnetic stirrer to ensure complete evaporation of dichloromethane, leaving NP suspension. The suspension was centrifuged at 10,000 rpm for 20 min, resulting in the formation of a pellet at the bottom of the tube. This pellet was washed with PBS, re-suspended and again centrifuged. The pellet was collected and allowed to dry completely. The powdered particles were collected, weighed and used for further evaluation.

Experimental design

Central composite rotatable design-response surface methodology (CCRD-RSM) was used to systemically investigate the influence of three critical formulation variables, drug polymer ratio, aqueous organic phase ratio, and sonication time on particle size, drug loading percentage

(%, w/w) and EE (%, w/w) of the prepared NPs. For each factor, the experimental range was selected on the basis of the results of preliminary experiments and the feasibility of preparing the NPs at the extreme values. The value range of the variables was drug polymer ratio (X1) of 1:1 to 1:4, aqueous organic phase ratio (X2) of 1:5 to 1:10 and sonication time (X3) of 10-30 min. A total of 20 tests were conducted.

Particle size, polydispersity index and zeta potential measurement

PZ and polydispersity indices (Pls) of silybin NPs were measured by dynamic light scattering using a 90 plus particle sizer (Master sizer, Malvern instruments, London, UK) equipped with MAS Option particle sizing software. The measurements were made at a fixed angle of 90° for all samples. The samples were suitably diluted with Milli Q water for every measurement. Zeta potential measurements were also made using an additional electrode in the same instrument. For zeta potential determination, samples of all formulations were diluted with 0.1 mM KCl and placed in the electrophoretic cell, where an electric field of about 15 V/cm was applied. The mean hydrodynamic diameter (Dh) and PI of the particles were calculated using the cumulative analysis after averaging the three measurements.

Transmission electron microscopy

Transmission electron microscopy (TEM) was performed using a Philips CM 10 transmission electron microscope. The sample was prepared by a formvar resin grid method. Briefly, 0.5% w/v suspension of silybin NPs was sprayed on a formvar resin coated TEM grid and air-dried for 10 min before observation. Contrast enhancement and particle measurement were performed using the National Institutes of Health image software.

Determination of drug loading and entrapment efficiency

Drug EE and DL of the prepared silybin NPs were determined by the following procedures: Firstly, a certain volume of NP suspension was accurately taken, dissolved and diluted with anhydrous methanol. Then, drug content in the resultant solution was determined by high performance liquid chromatography (HPLC) method and the calculated drug amount was designated as Wtotal. To determine the unencapsulated drug, equal volume of NP suspension was accurately taken and ultra-filtered by a filter membrane with molecular weight cut-off (MWCO) of 12 kDa (Reili Separation Instrument Factory, Shanghai, China). The ultra-filtrate was diluted with anhydrous ethanol and drug content in the resultant solution was analyzed under the same HPLC condition. The amount of free drug was designated as Wfree. Consequently, the drug EE and DL could be calculated by the following equations [31]:

$$EE\ (\%)=(W_{total}-W_{free})/W_{total}\times100 \quad \text{.....Equation 1}$$

$$DL\ (\%)=(W_{total}-W_{free})/W_{polymer}\times100 \quad \text{.....Equation 2}$$

where W_{total} was the total amount of drug, W_{free}

was the amount of unencapsulated drug, and $W_{polymer}$ was the weight of the polymer.

MTT assay

Evaluation of cytotoxicity was done using MTT (3-(4,5-dimethylthiazol-2-yl)-2, 5 diphenyltetrazolium bromide dye) assay in DLy and normal mouse bone marrow cells. DLy cells were harvested from DLy bearing mice and the mouse bone marrow cells were isolated from the femur bone of a normal adult mouse. Cells (2.5×10^4/mL) DLy cells and bone marrow cells (BMC) were seeded in RPMI 1640 medium (10% FBS and antibiotic solution) in a culture plate with saline, silybin and silybin NPs. The culture plates were incubated for 24 hrs at 37 °C and 5% CO_2. After incubation, 10 µL of MTT (5 mg/mL in PBS) were added to each well and incubated for an additional 2 hrs at 37 °C to allow intracellular reduction of the soluble yellow MTT to insoluble purple formazan crystals. These formazan crystals were dissolved in 100 µL of DMSO and incubated for 30 min at 37 °C [32]. The absorbance of the solution was read at 570 nm using a microplate reader (Microscan (MS5608A), India). Three independent experiments were carried out and 5 replicates were taken for each experiment. Percentage inhibition was considered by the formula given below:

$$\% \ inhibition = \frac{Control\ abs - Sample\ abs}{Control\ abs} \ x\ 100$$

Anticancer activity of silybin nanoparticles and silybin in DENA treated rats

Male Wistar rats (4-6 months old; weight: 0.155-0.175 kg) were housed in cages and kept on a 12-h light/dark cycle. After acclimatization, HCC was induced in rats by supplementation of 100 mg/L of DENA in drinking water for 8 weeks [33]. The rats (6-8 months old) were randomly divided into 3 groups (5 animals per group) and maintained for one week. After one week of DENA induction, saline, silybin and silybin NPs were administered orally with oral canula on days 1, 7, 14, 21, 28, 35, 42 and 49. During treatment, the weight of animals was monitored and the animals were sacrificed at the end of study under sodium pentabarbitrate anaesthesia. Tissues (liver, kidneys, heart and spleen) were collected and blood was drawn by puncturing the heart. Tumor nodules > 3 mm in diameter (measured with a digital caliper) were counted on the surface of each lobe of the liver and the variation in the nodule numbers amongst the 3 groups was statistically evaluated. To make neoplastic nodules more evident, further evaluation of tumor growth was performed by fixing the lobes in 10% formalin. The upper and lower surfaces of each fixed lobe, together with a millimeter-graded bar were photographed. To avoid uncertainty in the result, lumps smaller than 2 mm were excluded. The antitumor effect of the formulations was estimated by comparing the number of animals with more than 40 tumor lesions in each of the 3 experimental groups. Formalin-fixed lobes were embedded in paraffin and routinely stained with hematoxylin and eosin (H&E).

Statistics

The relationships between responses and formulation variables of all model formulations were studied by Design Expert ® 8.0.7.1 software. Statistical analyses, including stepwise linear regression and response surface analysis, were conducted. The significant terms ($p<0.05$) were chosen for final equations. Suitable models consisting of 3 components included linear, quadratic and special cubic models. The best-fitting mathematical model was selected, based on the comparisons of several statistical parameters, including the coefficient of variation (CV), the multiple correlation coefficients (R^2), and the adjusted multiple correlation coefficient (adjusted R^2) [34].

Results

Optimization of the formula

Table 1 shows the experimental results concerning the tested variables on drug EE, DL percentage, and mean diameter of particle size. The three dependent values ranged from 83.24 to 97.24%, 2.86 to 14.98% by weight and 242 to 370 nm. A mathematical relationship between factors and parameters was generated by response surface regression analysis using Design-Expert® 7.0 software. The 3D response surface graphs for the most statistical significant variables on the evaluated parameters are shown in Figure 1. The response surface diagrams showed that the higher the polymer concentration, the higher the EE, DL and the particle size. Furthermore, the particle size and EE significantly increased with increasing aqueous/organic phase ratio. The lack-of-fit was not significant at 95% confidence level. All the remaining parameters were significant at $p \leq 0.05$. The statistical analysis of the results generated the following polynomial equations:

$$EE = +107.6 - 1.158 \times A - 0.94 \times B + 3.54 \times C + 3.01 \times B \times C$$

$$DL = +8.34 + 2.88 \times A - 1.80 \times B - 0.63 \times C - 0.39 \times A \times B + 0.34 \times B \times C + 0.42 \times B2$$

$$PS = +300.10$$

where X1, X2 and X3 represent the coded values of the drug/polymer ratio, aqueous/organic phase ratio and sonication time, respec-

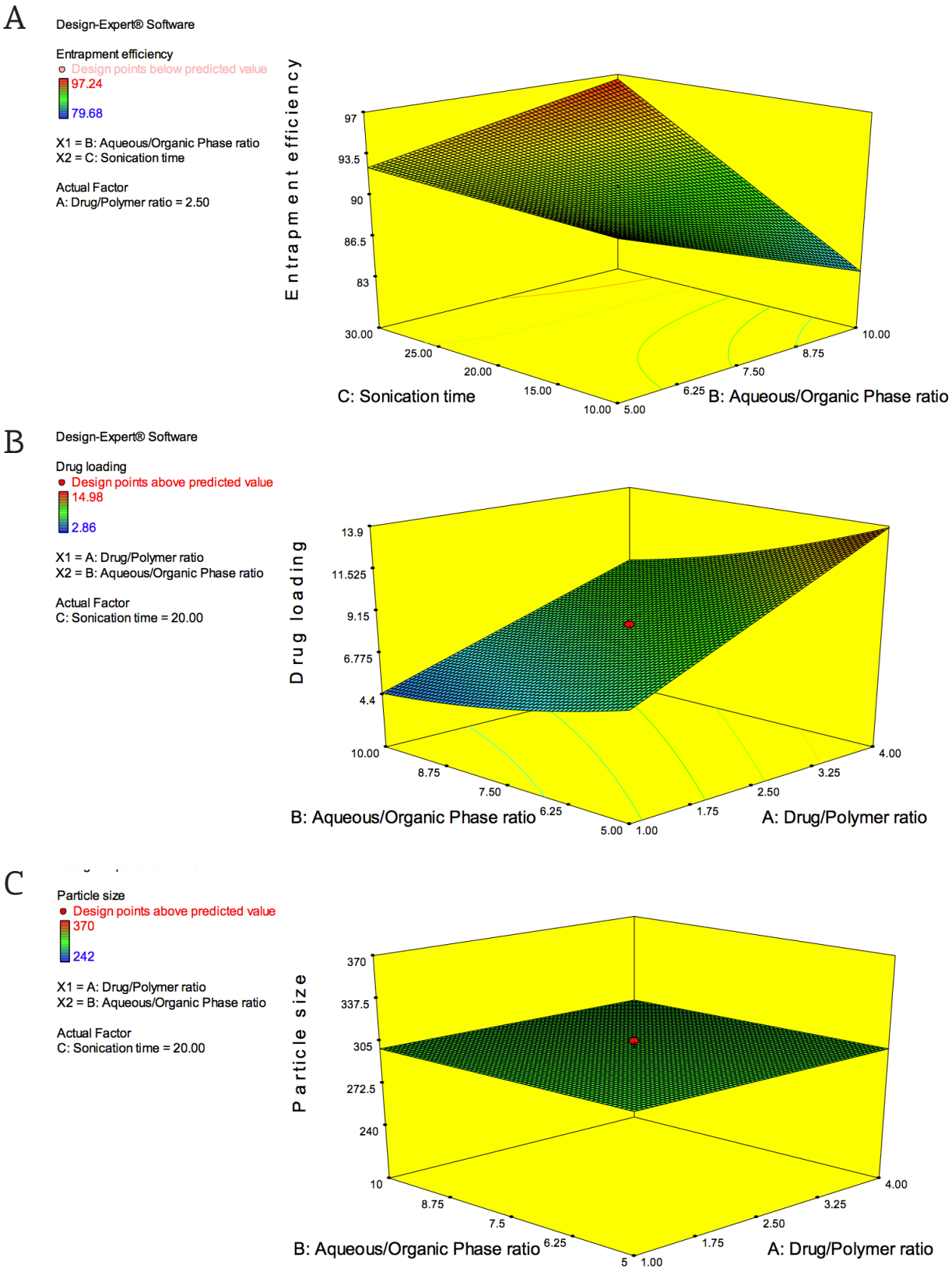

Figure 1. Three dimensional (3D) response surface plots showing the effect of the variable on the response. **(A)**: The effect of aqueous/organic phase ratio and sonication time on the entrapment efficiency; **(B)**: The effect of drug/polymer ratio and aqueous/organic phase ratio on the drug loading; **(C)**: The effect of aqueous/organic phase ratio and drug/polymer ratio on particle size.

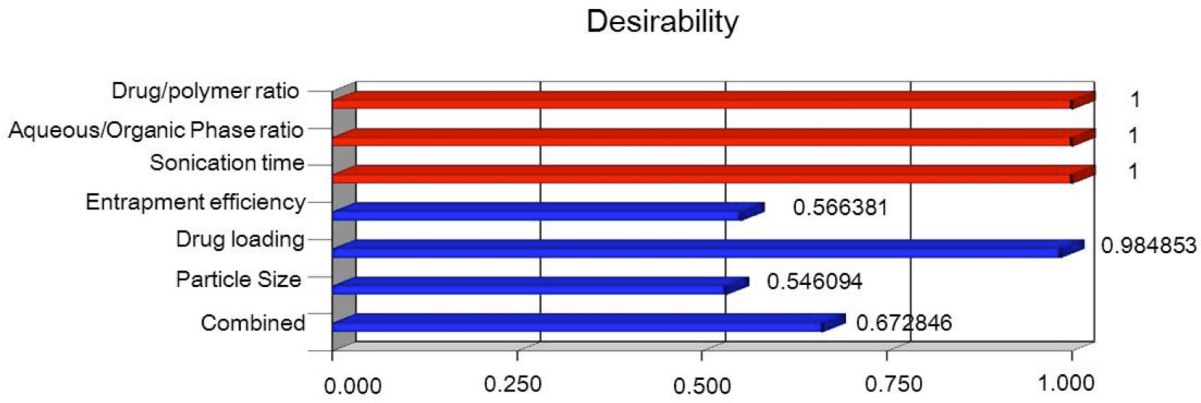

Figure 2. Graphical representation of the overall desirability function D (D=0.984).

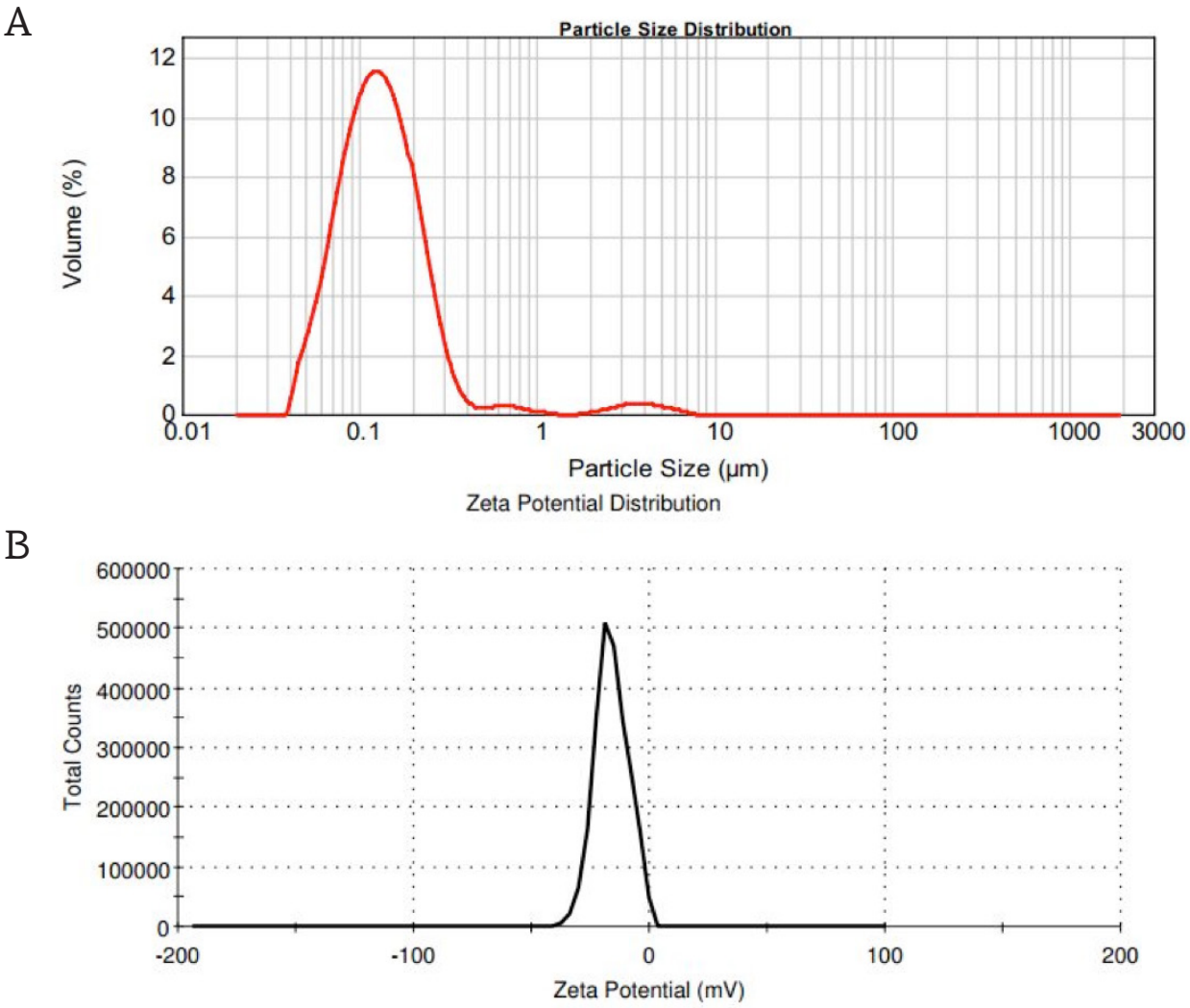

Figure 3. Particle size distribution **(A)** and zeta potential **(B)** of silybin nanoparticle. Mean particle size of silybin nanoparticle was found to be 216 nm and zeta potential -15mV.

tively. The fitting results indicated that the optimized nanoparticles with high EE, high DL percentage and small mean diameter was obtained at the drug/polymer ratio of 1:4, aqueous/organic phase ratio of 1:5 and sonication time of 10 min, respectively. Table 2 showed that the experimental values of the two batches prepared within the optimum range were very close to the predicted values, with low percentage bias, suggesting that the optimized formulation was reliable and

Table 1. Central composite design consisting of experiments for the study of three experimental factors in coded levels with experimental results

Formulation	Coded value variables			Response values		
	X_1	X_2	X_3	EE (%)	DL (%)	PS (nm)
1	-1	-1	-1	93.82	8.23	250
2	1	-1	-1	91.69	14.98	270
3	-1	1	-1	85.22	5.43	290
4	1	1	-1	79.68	9.82	320
5	-1	-1	1	94.43	6.54	252
6	1	-1	1	95.26	12.12	280
7	-1	1	1	97.24	4.29	282
8	1	1	1	95.89	9.12	310
9	-1	0	0	92.48	2.86	308
10	1	0	0	83.24	13.41	302
11	0	-1.682	0	89.95	12.84	370
12	0	1.682	0	92.54	6.08	350
13	0	0	-1.682	87.70	8.72	340
14	0	0	1.682	97.19	7.4	242
15	0	0	0	90.48	8.45	306
16	0	0	0	90.48	8.45	306
17	0	0	0	90.48	8.45	306
18	0	0	0	90.48	8.45	306
19	0	0	0	90.48	8.45	306
20	0	0	0	90.48	8.45	306

EE: entrapment efficiency, DL: drug loading, PS: particle size

Table 2. Comparison of experimental and predicted values under optimal conditions for final formulation

Drug/ Polymer ratio	Aqueous/ Organic phase ratio	Sonication time (min)	Particle size (nm)	Entrapment efficiency, %	Drug loading, %
1:4	1:5	10			
	Predicted		202	89	14
	Experimental		200	88	15
	Bias (%)		2	1	1
	Acceptance criteria = 2%				

Bias was calculated as (predicted value-experimental value)/predicted value ×100

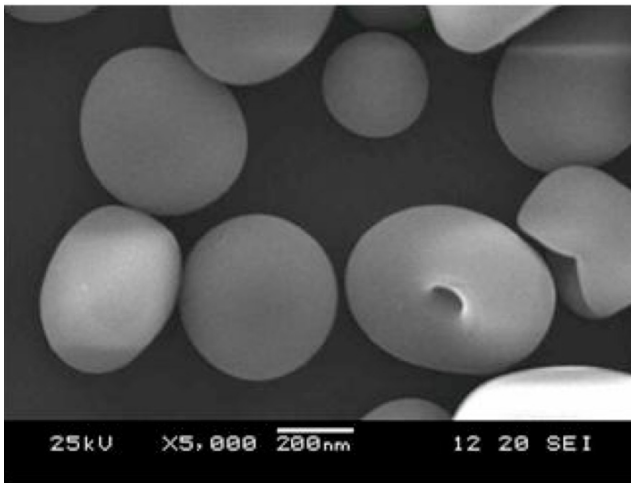

Figure 4. TEM of silybin nanoparticles.The silybin nanoparticles were spherical and had a size about 200 nm.

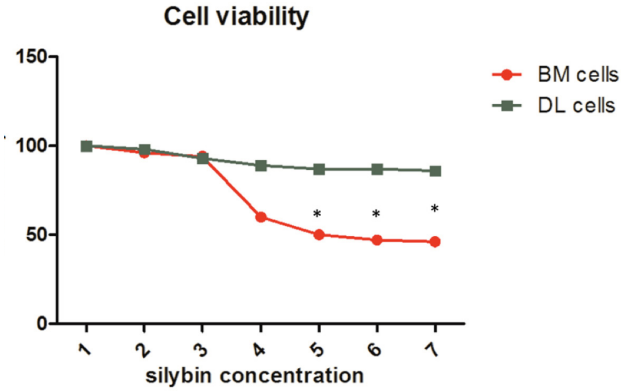

Figure 5. The graph displays the cytotoxicity profile of silybin nanoparitcles against DL cells and mouse bone marrow cells (BM cells) at increasing concentrations on 24-hr incubation. Results are expressed as a percentage of control ± standard error of the mean (SEM) from at least three independent experiments. *p < 0.05, compared with the control.

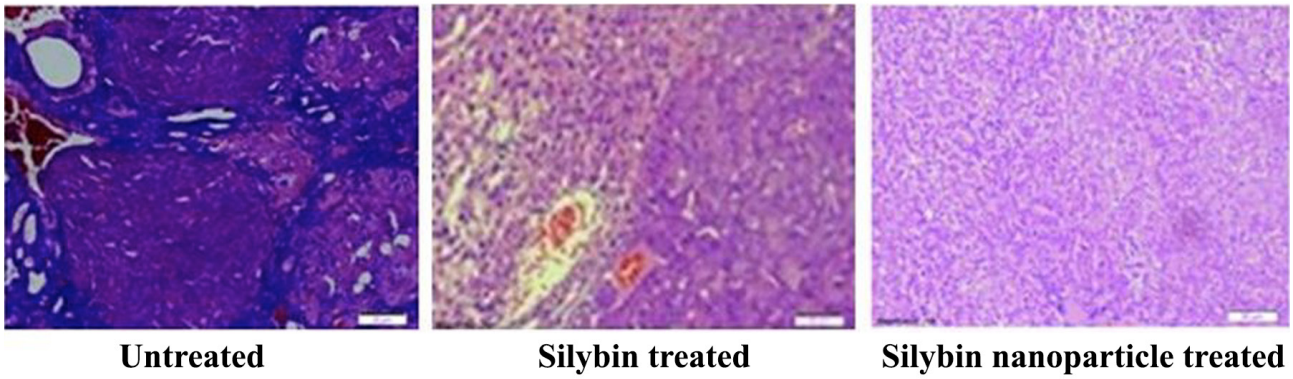

Figure 6. Hematoxylin and eosin staining of liver nodules according to treatments. Liver tissue sections showed normal cellular morphology.

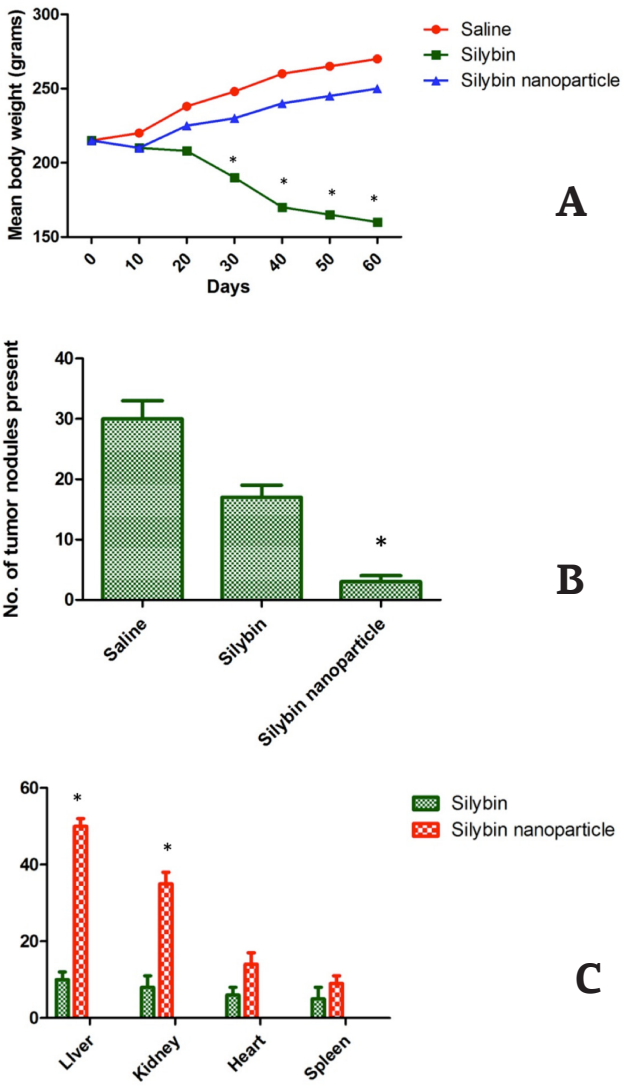

Figure 7. Effects of silybin nanoparticles. **A:** shows that the body weight of rats decreased significantly when treated with silybin and increased in saline-treated animals. When treated with silybin nanoparticles, a slight increase in body weight was observed. **B:** shows that tumor nodules on the surface of the liver were reduced to a large extent when treated with silybin nanoparticle. **C:** The highest level of silybin was found only in the liver of rats treated with nanoformulation due to their targeted delivery. *p < 0.05, compared with the control.

reasonable. The overall desirability (D) 0.984 observed is graphically shown in Figure 2.

Characterization

Particle size, polydispersity index and zeta potential measurement

The mean particle size of silybin NPs was 216 nm with a polydispersity index of 0.193 ± 0.026 (Figure 3). A narrow PI means that the colloidal suspensions are homogeneous in nature. The zeta potential of the silybin NP was found to be -15 mV, and it was sufficiently high to form stable colloidal nanosuspension.

Transmission electron microscopy

In order to provide information on the morphology and size of the optimal silybin NP, TEM was used to take photos of the optimal silybin NP, as shown in Figure 4. The silybin NPs were spherical and had a size about 216 nm. The diameter observed by TEM was smaller, while the diameter determined by dynamic light scattering (DLS) was above 200 nm. The reason may be that the two methods are based on different sample preparation processes.

MTT assay

The silybin NP was screened for its cytotoxicity by MTT assay in DLy cells and in normal mouse bone marrow cells. The silybin NP induced cytotoxic response against DLy cells (Figure 5). In the case for normal mouse bone marrow cells the silybin NP did not induce cytotoxicity. The vehicle group also did not show any effect in DLy cells (Figure 5).

The data obtained from the MTT assay clearly showed that silybin NP can potentially induce cytotoxicity in DLy cells without affecting the normal cells. Therefore, we finally showed that the silybin NP induced cytotoxic effect in DLy cells but failed to exert cytotoxicity in normal cells.

Treatment of hepatocellular carcinoma

HCC was induced by oral administration of DENA and was evidenced through the formation of nodules in the liver and also from the cancerous cellular growth profile in liver histochemical sections. In the case of rats treated with silybin, the nodule formation was found relatively reduced though some cancerous growth was still evident in liver sections (Figure 7 B). In contrast, in the group treated with silybin NPs the nodules in the liver were significantly reduced, suggesting highest inhibition of HCC when silybin loaded nanoformulations were employed (Figure 7 B). This was further confirmed by histochemical analysis, where the liver tissue sections showed normal cellular morphology (Figure 6). The above observations suggest that the silybin NP formulations were highly effective when compared to silybin.

Efficacy of nanoformulations

HCC bearing rats showed an increase in mean

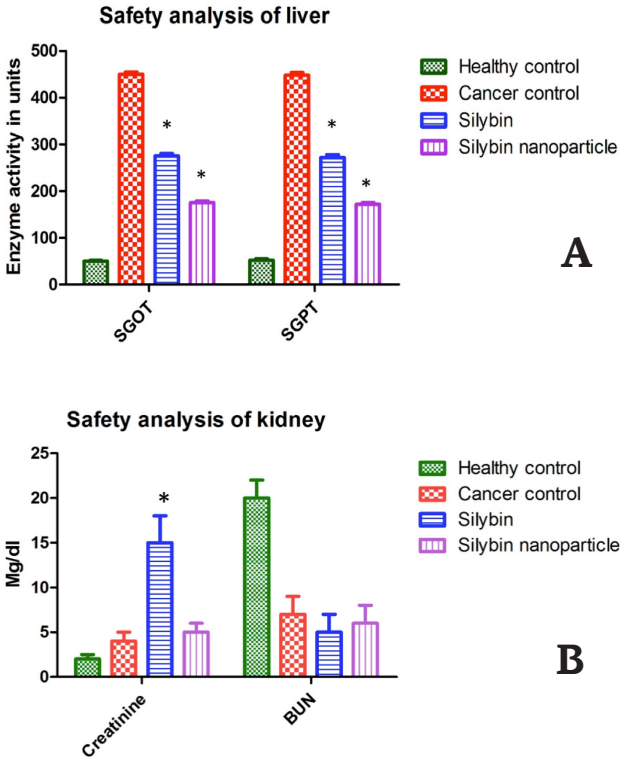

Figure 8. Safety analysis in treated rats. **A:** Kidney toxicity was evaluated by the levels of creatinine and blood urea nitrogen (BUN), whereas liver toxicity **(B)** was estimated via SGOT and SGPT levels. These 4 markers showed minimal levels in animals treated with silybin nanoformulation. *p < 0.05 compared with the control.

body weight (MBW), which was drastically reduced when treated with silybin, indicating the severe side effects exerted by the drug (Figure 7 A), whereas in the case of treatment with silybin NPs the MBW of animals was significantly restored (Figure 7 A) with a slight decrease in weight due to cancer inhibition. Thus, the NP encapsulation has reduced the silybin treatment-associated weight loss, demonstrating decreased side effects.

The concentration of silybin during treatment was estimated in the tissue homogenate prepared from liver, kidney, heart and the spleen of the treated rats. The results shown in Figure 7 C indicate that high levels of silybin were present in the liver, while the levels were significantly lower in the kidney, heart and spleen when administered through NPs. Since the liver is the site of action, the presence of higher drug levels in it when administered through NPs would help in enhancing the efficacy of treatment.

Safety profile

Non-specific toxicities of nanoformulations were analysed in tissue homogenates of the treated rats using specific-markers. After absorption from the GI tract the carrier molecule entered the liver and got excreted through the kidney. Here, the safety analysis for the kidney was done by estimating the parameters creatinine and blood urea nitrogen (BUN). Significant increase in creatinine levels and poor elimination of BUN indicated kidney damage which in the present study was evident in the silybin-treated rats (Figure 8 B). However, in the case of the rats treated with nanoformulations the safety parameters clearly indicated a significant reduction in the extent of the damage. Liver damage was analysed by estimating the levels of SGOT and SGPT which were found increased in case of silybin treatment and reduced substantially when treated with nanoformulations (Figure 8 A).

Discussion

Various nanoscale constructs and targets have been evaluated for specific targeting of HCC, with limited efficacy. This novel NP construct has a number of advantages in its design and application. First, our study clearly illustrates the ability of the silybin NPs to target HCC cells with high specificity. Second, the characteristics of the NP construct are optimal for targeted delivery to the cells of interest and an ideal target-specific imaging contrast agent in terms of particle size and zeta potential. The hydrodynamic size of 200 nm is large enough so that it will not be quickly filtered out through the glomeruli but small enough that it can evade the RES clearance by the EPR effect. A negative zeta potential also minimizes unwanted nonspecific binding and uptake by surrounding tissues and allows for deeper tissue penetration to the target [35]. It also offers potential use as a nanocarrier for HCC-targeted therapeutics, delivering drugs and other payloads. NPs have certain advantages such as maximal load of the drug and long shelf life. Furthermore, their body distribution and permeability in tissues can be controlled by size and surface properties [36]. Enhanced liver protection of curcumin, curcumin analogues and piperine, using Kupffer cell -targeted NP and liposomal formulations, and sustained-release intraperitoneal microspheres [37-39] has been reported. Silybin, a natural antioxidant, has long been used for the treatment of chronic liver diseases. Silybin was administered as nanoformulation to offer treatment as well as liver protection. It can also be targeted to Kupffer cells and its delivery into these cells can be enhanced with silybin encapsulated in particulate systems and

could further improve the therapy.

To achieve the aims of this study, silybin NPs have been prepared using the emulsion solvent evaporation technique optimizing the central composite rotatable design-response surface methodology. PZ and EE of silybin NPs increased with increase in polymer content. This may be due to the availability of more polymers to coat the drug.

Increase in matrix content is expected to raise the EE by providing more space to incorporate the drug. Increment of the lipid content also reduces the escaping of drug into the external phase, which accounts for an increase in EE [40]. EE significantly increased at increasing drug: lipid ratio, whereas with this increasing ratio, an increase in PS was observed. Numerous studies have reported that increasing lipid content results in larger particles and broader PS distribution [41]. Larger PS with an increase in lipid content could be attributed to decrease in emulsifying efficiency, increase in particle agglomeration, and increased drug loading as well. The ratio of oil phase and aqueous phase showed a great impact on the EE of the NPs. Increasing the aqueous phase volume results in an increase in EE. This could be due to lesser aggregation of the particles in a larger space. Different studies have shown that the aqueous phase volume has a paramount effect on the formation of NPs. In a recent study, with increased volume of aqueous phase, increase in drug content of particles prepared by homogenization and sonication was observed [42].

The efficacy and safety of the silybin when administered as NPs was studied. The efficacy of the oral nanoformulations of silybin was confirmed evidently from the number of nodules observed in the treated liver samples and also the mean body weight. The highest amount of silybin was found to be present in the liver when delivered through these nanoformulations, which points out to the efficient delivery of the drug to the target tissue.

The safety profile of the formulations in the treated rats was found to be similar to that of untreated rats. The efficacy of drug in nanoformulation was confirmed by the semi-quantitative analysis of molecular markers which showed significant enhancement in the rate of tumor suppression. This is further supported by the observed decreased vasculature around the tumor. While the results of the studies on small animals like rats are encouraging, further studies need to be undertaken, particularly in determining dosages in human studies.

Overall, the findings of this study suggest that the developed NP formulation may be useful in the treatment of HCC with silybin. It is likely that these results can be extrapolated to other drugs, suggesting the probability of nanoparticle passive targeting of drugs to the liver.

In summary, the results obtained involving *in vitro* and *in vivo* studies in DLy cells clearly demonstrated potent anticancer activity of silybin NP. This anticancer activity is due to apoptotic-inducing property and cell cycle delay with the silybin NP, thereby enhancing the survival of the tumor-bearing mice. The fundamental advantage of this silybin NP is that it exhibits high cytotoxicity in DLy cells without affecting normal cells. The results of the present study seem quite promising and should be followed by the identification of the molecular mechanism regulated by the silybin NP to combat other cancers.

Acknowledgement

This research was carried out in the laboratories department without any restrictions and has taken the help from many scientists from the department, hence we need to thank the department where the research was done.

Conflict of interests

The authors declare no confict of interests.

References

1. Sherman M. Hepatocellular carcinoma: epidemiology, surveillance, and diagnosis. Semin Liver Dis 2010;30:3-16.
2. Ferenci P, Fried M, Labrecque D. Hepatocellular carcinoma (HCC): a global perspective. J Clin Gastroenterol 2010;44:239-245.
3. Caldwell S, Park SH. The epidemiology of hepatocellular cancer: from the perspectives of public health problem

to tumor biology. J Gastroenterol 2009;44:96-101.

4. Altekruse S, McGlynn K, Reichman M. Hepatocellular carcinoma incidence, mortality, and survival trends in the United States from 1975 to 2005. J Clin Oncol 2009;27:1485-1491.
5. Cabibbo G, Enea M, Attanasio M. A meta-analysis of survival rates of untreated patients in randomized clinical trials of hepatocellular carcinoma. Hepatology 2010;51:1274-1283.
6. Llovet J, Ricci S, Mazzaferro V. Sorafenib in advanced hepatocellular carcinoma. N Engl J Med 2008;359:378-390.
7. Bruix J, Llovet J. Major achievements in hepatocellular carcinoma. Lancet 2009;373:614-616.
8. Massarweh N, Park J, Farjah F. Trends in the utilization and impact of radiofrequency ablation for hepatocellular carcinoma. J Am Coll Surg 2010;210:441-448.
9. Bruix J, Sherman M. Practice Guidelines Committee, American Association for the Study of Liver Diseases. Management of hepatocellular carcinoma. Hepatology 2005;42:1208-1236.
10. Ayyappan A, Jhaveri K. CT and MRI of hepatocellular carcinoma:an update. Expert Rev Anticancer Ther 2010;10:507-519.
11. Sangiovanni A, Manini M, Iavarone M. The diagnostic and economic impact of contrast imaging techniques in the diagnosis of small hepatocellular carcinomas in cirrhosis. Gut 2010;59:638-644.
12. Silva M, Hegab B, Hyde C. Needle track seeding following biopsy of liver lesions in the diagnosis of hepatocellular cancer: a systematic review and meta-analysis. Gut 2008;57: 1592-1596.
13. Saborido B, Diaz J, de Los Galanes S. Does preoperative fine needle aspiration-biopsy produce tumor recurrence in patients following liver transplantation for hepatocellular carcinoma? Transplant Proc 2005;37:3874-3877.
14. Veiseh O, Sun C, Fang C. Specific targeting of brain tumors with an optical/magnetic resonance imaging nanoprobe across the blood-brain barrier. Cancer Res 2009;69:6200-6207.
15. Zhang Y, Sun C, Kohler N. Self-assembled coatings on individual monodisperse magnetite nanoparticles for efficient intracellular uptake. Biomed Microdevices 2004;6:33-40.
16. Kievit F, Veiseh O, Bhattarai N. PEI-PEG-chitosan copolymer coated iron oxide nanoparticles for safe gene delivery: synthesis, complexation, and transfection. Adv Funct Mater 2009;19:2244-2251.
17. Ruoslahti E, Bhatia S, Sailor M. Targeting of drugs and nanoparticles to tumors. J Cell Biol 2009;188:759-768.
18. Harris T, von Maltzahn G, Lord M. Protease-triggered unveiling of bioactive nanoparticles. Small 2008;4:1307-1312.
19. Moghimi S, Hunter A, Murray J. Long-circulating and target specific nanoparticles: theory to practice. Pharmacol Rev 2001;53:283-318.
20. Schipper M, Iyer G, Koh A. Particle size, surface coating, and PEGylation influence the biodistribution of quantum dots in living mice. Small 2009;5:126-134.
21. Lee H, Lee E, Kim K. Antibiofouling polymer-coated superparamagnetic iron oxide nanoparticles as potential magnetic resonance contrast agents for in vivo cancer imaging. J Am Chem Soc 2006;128:7383-7389.
22. Chen J, Wu H, Han D. Using anti-VEGF McAb and magnetic nanoparticles as double-targeting vector for the radioimmunotherapy of liver cancer. Cancer Lett 2006;231:169-175.
23. Liu P, Li Z, Zhu M. Preparation of EGFR monoclonal antibody conjugated nanoparticles and targeting to hepatocellular carcinoma. J Mater Sci Mater Med 2010;21:551-556.
24. Kou G, Wang S, Cheng C. Development of SM5-1-conjugated ultrasmall superparamagnetic iron oxide nanoparticles for hepatoma detection. Biochem Biophys Res Commun 2008;374:192-197.
25. Kim T, Park I, Nah J. Galactosylated chitosan/DNA nanoparticles prepared using water-soluble chitosan as a gene carrier. Biomaterials 2004;25:3783-3792.
26. Sharkey R, Cardillo T, Rossi E. Signal amplification in molecular imaging by pretargeting a multivalent, bispecific antibody. Nat Med 2005;11:1250-1255.
27. Goldenberg DM, Sharkey RM, Paganelli G. Antibody pretargeting advances cancer radioimmunodetection and radio-immunotherapy. J Clin Oncol 2006;24:823-834.
28. Box GEP, Hunter JS. Multi-factor experimental design for exploring response surfaces. Ann Math Statistics 1975;28:195-241.
29. Kassama LS, Shi J, Mittal GS. Optimization of supercritical fluid extraction of lycopene from tomato skin with central composite rotatable design model. Separation Purification Technol 2008;60:278-284.
30. Chakrabarti S, Chakrabarti A, Pal AK. Chromosome analysis of Dalton's lymphoma adapted to the Swiss mouse: clonal evaluation and C-heterochromatin distribution. Cancer Genetics Cytogenetics 1984;11:417-423.
31. Liu H, Gao C. Preparation and properties of ionically cross-linked chitosan nanoparticles. Polym Adv Technol 2009;20:613-619.
32. Mosmann T. Rapid colorimetric assay for cellular growth and survival: application to proliferation and cytotoxicity assays, J Immunol Meth 1983;65:55-63.
33. Fiume L, Bolondi L, Busi C, Chieco P, Kratz F. Doxorubicin coupled to lactosaminated albumin inhibits the growth of hepatocellular carcinomas induced in rats by diethylnitrosamine. J Hepatol 2005;43:645-652.
34. Myers RH, Montgomery DC. Response Surface Methodology. John Wiley & Sons Inc, New York, 1995.
35. Kim B, Han G, Toley B. Tuning payload delivery in tumour cylindroids using gold nanoparticles. Nat Nanotechnol 2010;5:465-472.
36. Stayton PS, Hoffman AS, Murthy N et al. Molecular engineering of proteins and polymers for targeting and intracellular delivery of therapeutics. J Control Release 2000;65:203-220.
37. Bonepally CR, Aukunuru JV, Yellu NR, Vanga MR. Fabrication and Investigations on Hepatoprotective Activity of Sustained Release Biodegradable Piperine Microspheres. Int J Pharm Sci Nanotech 2008;1:87-96.

38. Anuradha CA, Aukunuru J. Preparation, characterization and in vivo evaluation of Bis-demethoxy curcumin analogue (BDMCA) nanoparticles. Trop J Pharm Res 2010;9:51-58.
39. Konatham S, Nyathani H, Bonepally CR, Yeannameneni P, Aukunuru J. Liposomal delivery of curcumin to liver. Turk J Pharm Sci 2010;7:89-98.
40. Shah KA, Date AA, Joshi MD, Patravale VB. Solid lipid nanoparticles (SLN) of tretinoin: potential in topical delivery. Int J Pharm 2007;2:163-171.
41. Trotta M, Debernardi F, Caputo O. Preparation of solid lipid nanoparticles by a solvent emulsification-diffusion technique. Int J Pharm 2003;2:153-160.
42. Budhian A, Siegel SJ, Winey KI. Haloperidol-loaded PLGA nanoparticles: systematic study of particle size and drug content. Int J Pharm 2007;2:367-375.